JOURNAL OF GEOPHYSICAL RESEARCH, VOL. 104, NO. D11, PAGES 13,993–14,002, JUNE 20, 1999

Satellite observations of temporary and irreversible denitrification

A. E. Dessler[1] and J. Wu

Earth System Science Interdisciplinary Center and Department of Meteorology, University of Maryland, College Park

M. L. Santee

NASA Jet Propulsion Laboratory, Pasadena, California

M. R. Schoeberl

NASA Goddard Space Flight Center, Greenbelt, Maryland

Abstract. We have investigated temporary and irreversible denitrification in the polar regions. We find that the formation of type I polar stratospheric clouds (PSCs) in both hemispheres is best described by a supercooled ternary solution model. Considering the uncertainties in the analysis, our results are also consistent with a nitric acid dihydrate composition for type I PSCs, but not a nitric acid trihydrate composition. In the Northern Hemisphere, we observe that an upper limit of 17% of HNO_3 is irreversibly lost each time the temperature of an air mass drops below ~190 K. It seems likely that in order to remove a significant fraction of the HNO_3 from an air mass in the Northern Hemisphere, one must expose it to low temperatures multiple times.

1. Introduction

In the wintertime polar lower stratosphere, the vast majority of total odd nitrogen ($NO_y \approx HNO_3 + ClONO_2 + 2xN_2O_5 + NO_2 + NO + NO_3$) is in the form of nitric acid HNO_3 [*Kawa et al.*, 1992a]. As the temperature decreases below ~196 K, the HNO_3 condenses into solid or liquid particles and is thereby removed from the gas phase. If the particles formed are large (radius > a few μm), then they settle to lower altitudes, possibly even out of the stratosphere. This process, which permanently removes the HNO_3 from the air mass, is generally referred to in the literature as "denitrification." In this paper, we will refer to this process as "irreversible denitrification." This will allow us to draw a distinction with the case where the particles formed are small (radius < a few μm), and they do not sediment. When the air parcel warms up, the HNO_3 contained in the particles is released back into the gas phase. We define a new term, "temporary denitrification," to refer to this latter process. The processes that regulate HNO_3 are important because the abundance of HNO_3 is generally thought to be one of the crucial factors that determine the amount of polar ozone loss during the late winter and early spring [e.g., *Brune et al.*, 1991; *Salawitch et al.*, 1993].

Previous work has highlighted important aspects of the microphysical basis of denitrification. It is now believed that there are two types of polar stratospheric cloud (PSC), designated type I and type II. Type I PSCs form at, or a few degrees below, 196 K, and are further subdivided into two primary classes. The first, designated type Ia, is a solid. These particles are likely crystalline nitric acid trihydrate ($HNO_3 \cdot 3H_2O$), also known as NAT, or crystalline nitric acid dihydrate ($HNO_3 \cdot 2H_2O$), also known as NAD. The other, designated type Ib, is thought to be liquid $H_2O/HNO_3/H_2SO_4$ aerosol, also referred to as supercooled ternary solution or STS. These type Ib particles are probably stratospheric sulfate aerosols (composed principally of H_2O and H_2SO_4) which have absorbed significant amounts of HNO_3 at temperatures below ~196 K (at ~50 hPa) [e.g., *Carslaw et al.*, 1997; *Tabazadeh et al.*, 1994].

The relative prevalence of these two types of PSC is currently unknown, although there is a growing body of evidence supporting the more frequent occurrence of type Ib [e.g., *Tabazadeh et al.*, 1994; *Drdla et al.*, 1994; *Toon and Tolbert*, 1995; *Massie et al.*, 1997; *Dye et al.*, 1996; *Santee et al.*, 1998]. Other forms of type I PSCs have also been suggested, but these are speculative and will not be considered in this paper.

Measurements of type I PSCs reveal characteristic radii of a micron or so [*Toon et al.*, 1990]. Such small particles have small settling velocities and therefore sedimentation of these particles is negligible (temporary denitrification). It is possible, however, that growth of a small number of type I PSCs could result in larger particles and subsequent sedimentation [e.g., *Drdla and Turco*, 1991] (irreversible denitrification). Because gas phase $[HNO_3]/[H_2O] \approx 10^{-3}$, type I PSC particles contain a small fraction of the available water vapor, so irreversible denitrification from sedimentation of these particles would not be accompanied by dehydration. This phenomenon, denitrifi-

[1]Also at NASA Goddard Space Flight Center, Greenbelt, Maryland

Paper number 1999JD900133.
0148-0227/99/1999JD900133$09.00

cation without dehydration, has been observed in the Arctic [*Fahey et al.*, 1990a], although the mechanism through which it arises is still a matter of debate.

Type II PSCs form at or just below the frost point, which, for typical lower stratospheric values, is ~189 K. These clouds are primarily water ice but also contain HNO_3 [*Kawa et al.*, 1992b]. Type II PSCs are predicted to have characteristic radii of 5-20 μm [e.g., *Panegrossi et al.*, 1996; *Drdla and Turco*, 1991], much larger than the type I PSC particles, and so will almost certainly experience significant sedimentation during their lifetimes. The sedimentation of these particles leads to both irreversible denitrification and dehydration, as has been observed in the Antarctic [*Fahey et al.*, 1990a]. For a review of PSCs, see *Peter* [1997], *World Meteorological Organization* [1995, section 3.3.1], *Santee et al.* [1998], and references therein.

The removal of gas phase HNO_3 (hereinafter $HNO_3(g)$) as the temperature of an air mass drops below ~196 K has been identified in satellite measurements [*Santee et al.*, 1995; 1996; 1997]. A shortcoming of these satellite data, however, is that the HNO_3 measurements are sensitive to $HNO_3(g)$ only. As a result, these data, by themselves, are unable to determine whether the the denitrification is temporary or irreversible.

The in situ NO_y instrument onboard NASA's ER-2 high-altitude aircraft is sensitive to both gas and particle phase HNO_3, and therefore can determine if HNO_3 has been permanently removed from an air mass [*Fahey et al.*, 1989]. Data from this instrument package have identified irreversible denitrification in both hemispheres. Irreversible denitrification is prevalent in the southern hemisphere [e.g., *Fahey et al.*, 1990a], where it is held to be a factor in the development of the Antarctic "ozone hole" [e.g., *Anderson et al.*, 1991; *Solomon*, 1990]. In the northern hemisphere, irreversible denitrification has been observed [*Kondo et al.*, 1992; *Fahey et al.*, 1990a; *Hintsa et al.*, 1998] but appears to be a rarer event. Unfortunately, the limited coverage of in situ instruments (in both time and space) makes it difficult to draw quantitative conclusions about the amount of denitrification in the northern polar region as a whole.

As a result, significant uncertainty concerning denitrification still exists. In this paper, we present calculations using satellite measurements of $HNO_3(g)$ abundances and extinction in combination with trajectory calculations to observe temporary and irreversible denitrification as air masses cool and then warm.

2. Data

Measurements utilized in this paper were made by instruments onboard the Upper Atmosphere Research Satellite (UARS) [*Dessler et al.*, 1998]. Measurements of HNO_3 abundances (version 4) were made by the Microwave Limb Sounder (MLS) at 100, 46, and 22 hPa, with precisions of 2.0, 3.0, and 4.5 ppbv, respectively. Preliminary comparisons with UARS Cryogenic Limb Array Etalon Spectrometer (CLAES) HNO_3 measurements indicate that MLS HNO_3 agrees well at 100 hPa but are usually 0-2 ppbv lower at 46 hPa and 0-4 ppbv higher at 22 hPa. However, while biases exist, there is good correspondence in the overall morphology of the HNO_3 fields. For more information about MLS HNO_3 data, see *Santee et al.* [1998].

Measurements of acrosol extinction at 780 cm^{-1} (12.8 μm) were made by the CLAES at 100, 68, 46, and 32 hPa. We will use version 8 of the data; detailed error analyses for version 7 of these measurements are presented by *Massie et al.* [1996]. Extinction at 780 cm^{-1} is most sensitive to particles with radii of several microns. In this paper, we will be using the extinction data as a qualitative indicator of the presence of PSCs in an air mass.

Trajectory calculations are made by the Goddard trajectory model [*Schoeberl and Sparling*, 1995]. Briefly, given an initial position of a 'parcel' in the atmosphere, the trajectory model uses horizontal wind velocity fields from the United Kingdom Meteorological Office (UKMO) [e.g., *Swinbank and O'Neill*, 1994] or the National Center for Environmental Prediction (NCEP) Climate Prediction Center to calculate the position of this parcel as a function of time. For computational simplicity, the trajectories are isentropic — i.e., they conserve their potential temperature. The errors in predicted position associated with trajectory calculations have been discussed in the literature [*Schoeberl and Sparling*, 1995; *Morris et al.*, 1995]. We use trajectories of several days or less in order to minimize errors.

Temperature plays a crucial role in this analysis and we use temperatures from the UKMO and NCEP in this paper. The uncertainties of these temperature fields are discussed by *Manney et al.* [1996].

3. PSC Formation

To study the formation of polar stratospheric clouds (PSCs) and the associated denitrification, we identify trajectories along which several measurements of HNO_3 and extinction were made. By observing the decrease in HNO_3 and increase in extinction as the temperature of the air parcel drops, we gain insight into the composition of the PSCs.

To find trajectories on which there are several UARS measurements of HNO_3 and extinction, we adapt the trajectory-mapping technique of *Morris et al.* [1995], which has been used successfully to compare noncollocated satellite measurements [*Dessler et al.*, 1995; *Morris et al.*, 1997]. Briefly, given a set of UARS measurements made over a range of several days, a parcel is initialized at the location and time of each measurement and trajectories are run isentropically (either forward or backward) to a common stopping time. Trajectories that are "near" each other at this stopping time are assumed to have been made in the same air mass at different times. In this paper, we define "near" to be 400-km distance and a difference of Ertel's potential vorticity of less than 1×10^{-5} m^2 K s^{-1}.

This procedure is shown schematically in Figure 1. The triangles represent measurements made on a certain day, while the circles represent measurements made during a subsequent day. Parcels initialized at the location and time of the measurements are advected to a common stopping time. From these six measurements, there is one match: the trajectories originating at the northernmost triangle and southernmost circle end up near each other. These measurements, made some time apart, are therefore assumed to

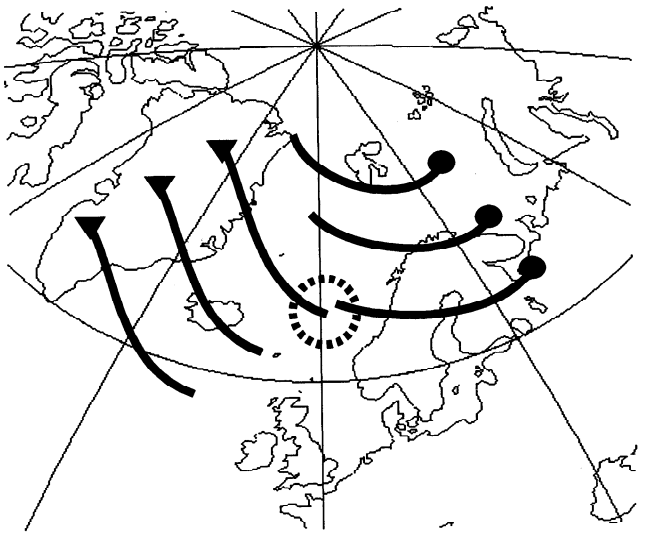

Figure 1. Schematic view of the method used to find UARS measurements made in the same air mass. The triangles represent measurements made on a certain day, and the circles represent measurements made on a subsequent day. Trajectories initialized at the measurement locations of UARS data are advected to a common stopping time; the solid lines indicate the paths of the trajectories. The locations of the parcels at the common stopping time are compared to find pairs that are "nearby." The dotted circle represents the nearness criteria. See text for more discussion.

be in the same air mass and can be compared to each other to study the evolution of the measured quantity over the time between the measurements. By including more days of data, we can find several measurements made over several days in the same air mass.

To study PSC formation, UARS data from four consecutive days are first interpolated to the 465-K potential temperature surface (~20 km) using UKMO or NCEP temperature fields. For each UARS measurement that is poleward of 60° in the hemisphere of interest, a parcel is initialized at the location and time of the UARS measurement, and trajectories are run to a common stopping time: midnight between the middle two days: e.g., if the 4 days being considered are January 6-9, then the stopping point is 0000UT, January 8.

From these trajectories, we find groups of measurements made over these 4 days that are in the same air mass. We take those groups of measurement which include a measurement made on the fourth day (in our example, January 9). For each group, we define the HNO_3 abundance on the fourth day as M_{final}. The average of the HNO_3 abundances from the first 3 days that were measured at temperatures above 196 K are defined to be $M_{initial}$. Because $M_{initial}$ values are derived from measurements made at temperatures above 196 K, we expect all of the HNO_3 in the air mass to be in the gas phase.

We then run the process above for every day between December 12 and March 28 of the year in question. In other words, we run the process for the first 4 days, December 12-15, and obtain the set of $M_{initial}$ and M_{final} values for these 4 days. Then, we increment the starting day and run the process for December 13-16, and repeat until the end of March is reached. We then combine all of the $M_{initial}$ and M_{final} values to obtain one set of $M_{initial}$ and M_{final} values for the entire winter.

We first apply this procedure to MLS measurements of HNO_3. Figure 2 shows the difference $M_{initial}$ - M_{final} for HNO_3 measurements plotted against the temperature of the M_{final} measurement for the Northern Hemisphere winter of 1995-1996. The points in Figure 2 are the individual differences, the solid line is an average of these points. The scatter in the points arises from precision uncertainty of the measurement, random error in the trajectories, and atmospheric variability. It is impossible to determine how much of the scatter is due to nonatmospheric sources. We do not, therefore, attempt to interpret the scatter as indicative of any atmospheric processes.

At M_{final} temperatures of 196 K and above, the average difference between HNO_3 at $M_{initial}$ and M_{final} is approximately zero. This is expected because at these temperatures, NAT and NAD do not form for stratospheric abundances of HNO_3 and H_2O, and STS particles absorb little HNO_3. Therefore we expect the HNO_3 at the beginning and end of the trajectories to be the same. As the M_{final} temperatures decrease below 196 K, Figure 2 shows average $M_{initial}$ - M_{final} increase, so there is less $HNO_3(g)$ at M_{final} than at $M_{initial}$. By M_{final} temperatures of ~187 K, virtually all of the HNO_3 in an air mass has been incorporated into solid or liquid particles. The dashed line, the average $HNO_3(g)$ at $M_{initial}$, shows an approximately constant value for $M_{initial}$ HNO_3 of ~11 ppbv.

In Figure 3 we plot the ratio of the solid to the dashed line from Figure 2. This can be thought of as the average fractional denitrification, i.e., the fraction of $HNO_3(g)$ that has been removed by incorporation into particles. Values near zero, which occur at temperatures above ~196 K, suggest that none of the HNO_3 has been removed from the gas phase. Values near 1, which occur at ~187 K, suggest that removal of $HNO_3(g)$ is essentially complete, with no HNO_3 left in the gas phase. Also shown in Figure 3 are the ratios from the Northern Hemisphere winters of 1991-1992, 1992-1993, and 1993-1994, as well as the calcula-

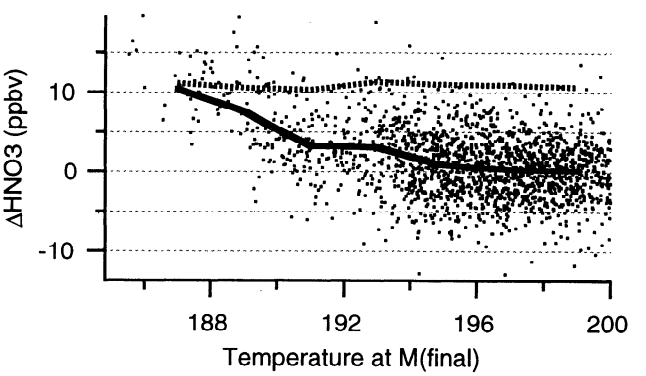

Figure 2. $M_{initial}$-M_{final} HNO_3 versus temperature of the air mass at M_{final} (dots), $M_{initial}$-M_{final} HNO_3 sorted into 2-K M_{final}-temperature bins and averaged (solid line), $M_{initial}$ HNO_3 sorted into 2-K M_{final}-temperature bins and averaged (dashed line). The analysis was run at 465-K potential temperature (~20 km), and between December 12, 1995 and March 28, 1996. Winds and temperatures are from the UKMO.

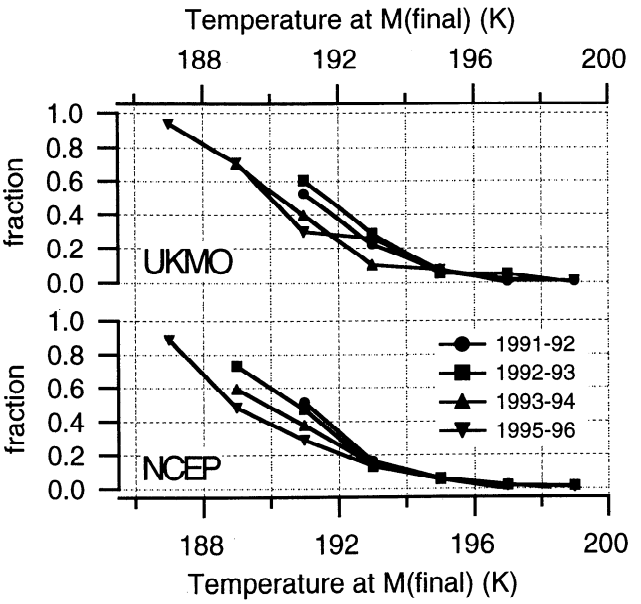

Figure 3. Ratio of average $M_{initial}$-M_{final} HNO_3 to average $M_{initial}$ HNO_3 plotted against the temperature of the air mass at the M_{final} location (i.e., ratio of solid line to dashed line in Figure 2). This can be interpreted as the average fractional HNO_3 depletion at a given M_{final} temperature. Analyses were run at 465-K potential temperature (~20 km), and between December 12 and March 28 of the years indicated. Winds and temperatures are from (top) the UKMO and (bottom) the NCEP.

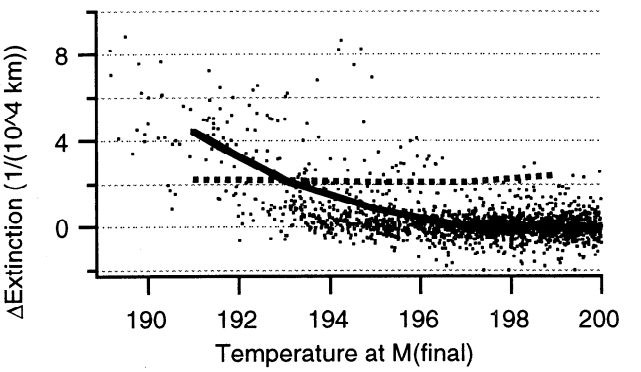

Figure 4. M_{final} - $M_{initial}$ extinction (at 780 cm^{-1}) versus temperature of the air mass at M_{final} (dots), M_{final} - $M_{initial}$ extinction (at 780 cm^{-1}) sorted into 2-K M_{final} bins and averaged (solid line), and $M_{initial}$ extinction sorted into 2-K M_{final} bins and averaged (dashed line). The analysis was run at 465-K potential temperature (~20 km), and between December 12, 1991 and March 28, 1992. Winds and temperatures are from the UKMO.

tions made using the NCEP winds and temperatures. In general, the UKMO- and NCEP-based analyses agree well.

All four of the winters show the same general pattern: no denitrification above 196 K, with denitrification increasing as the M_{final} temperature drops below 196 K. The analysis also shows a significant interannual variability. In the early years (1991-1992, 1992-1993), there is more denitrification at a given temperature than in later years (1993-1994, 1995-1996). This is discussed further below.

This analysis shows only that HNO_3 is removed from the gas phase. There is no information about whether the denitrification is temporary or irreversible. In other words, this analysis does not tell us if the HNO_3 will be returned to the gas phase when the air mass warms up (temporary denitrification) or if the particles have sedimented and permanently removed the HNO_3 (denitrification). This issue will be addressed in the second half of this paper.

We also have applied the same procedure to CLAES measurements of 780 cm^{-1} extinction along the trajectory. Figure 4 shows the results for the northern hemisphere winter of 1991-1992 at 465-K potential temperature. The points are individual measurements of M_{final} - $M_{initial}$ plotted against the temperature of the M_{final} measurement (note that in Figure 2, it was $M_{initial}$ - M_{final}); the solid line is an average of these points. The dashed line is an average of $M_{initial}$ as a function of the air parcel temperature at M_{final}. Note that the MLS and CLAES instruments make collocated measurements. Therefore individual points in Figure 4 correspond to those in Figure 2.

For M_{final} temperatures above ~196 K there is no difference between extinction at $M_{initial}$ and M_{final}, indicating no growth of PSCs at these temperatures. Below ~196 K, the difference in extinction between the $M_{initial}$ and M_{final} measurements increases as the temperature decreases, indicating an increase in the size and/or number of particles. Such a change is consistent with the growth of the particles by incorporation of HNO_3 (Figure 2). The behavior of these two geophysical parameters agrees with our present understanding of the thermodynamics of PSCs, and their consistency strongly suggests that we are in fact observing the growth of PSCs. While we have not attempted it in this

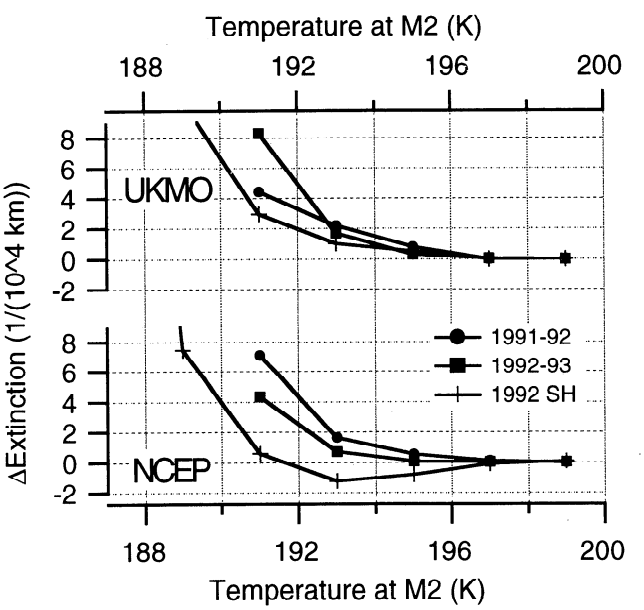

Figure 5. M_{final} - $M_{initial}$ extinction (at 780 cm^{-1}) sorted into 2-K M_{final} bins and averaged. The analyses were run at 465-K potential temperature (~20 km). Northern Hemisphere cases were run between December 12 and March 28 of the years indicated, the Southern Hemisphere case was run between June 12 and June 30, 1992. Winds and temperatures are from (top) the UKMO and (bottom) the NCEP.

paper, it is possible that a comparison between extinction calculations using assumed particle parameters and these extinction measurements could provide additional information about the composition of the particles.

In Figure 5 we plot the average difference between the extinction at M_{initial} and M_{final} (i.e., the solid line from Figure 4) for both winters in which the CLAES observed the Northern Hemisphere. The behavior of the two winters is generally similar, with both winters showing a rapid rise in extinction as the M_{final} temperature dropped below about 194 K.

Also shown is a similar calculation for the Southern Hemisphere winter of 1992. At the same temperature, the increase in extinction from M_{initial} to M_{final} tends to be smaller in the Southern Hemisphere than the Northern Hemisphere. The reasons for this hemispheric difference are not known. One unexpected feature is the slight decrease in extinction as temperatures decrease from 196 to 192 K in the NCEP analysis. Because it does not also occur in the UKMO analysis, we believe this feature is likely due to errors in the NCEP Antarctic winds.

We plot in Figure 6 the observed temperature dependence of the denitrification from three different STS models, a NAD model, and a NAT model at 465 K (the NAT and NAD parameterizations are from *Del Negro et al.* [1997], which is based on the work of *Hanson and Mauersberger* [1988], and *Worsnop et al.* [1993], the STS parameterization is from *Carslaw et al.* [1995]). NAT becomes thermodynamically stable and begins to form around 196 K (for HNO_3 of 12 ppbv and H_2O of 4.5 ppmv). Virtually all of the HNO_3 has been removed from the gas phase by ~192 K. The shape of the NAD curve is similar to the NAT curve, but offset by ~2-3 K; i.e., NAD starts forming at around 194 K, and virtually all of the HNO_3 is incorporated into particles by ~189 K.

There are three STS models in Figure 6, with the amount of H_2SO_4 varying between the models. The background STS model uses H_2SO_4 of 0.2 ppbv, corresponding to nonvolcanic abundances of stratospheric sulfate [*Weisenstein et al.*, 1997, Figure 1b]. The volcanic STS model uses H_2SO_4 of 1.5 ppbv, corresponding to a moderate volcanically perturbed environment. The super-volcanic STS model uses H_2SO_4 of 4.5 ppbv, corresponding to a heavily perturbed environment (D. K. Weisenstein, personal communication, 1998). HNO_3 and H_2O are the same as for the NAT and NAD models. At a given temperature, all three STS models show less denitrification than the NAT or NAD models. The STS models show the denitrification starts between 191 and 195 K, with increasing H_2SO_4 abundances correlated with increasing denitrification.

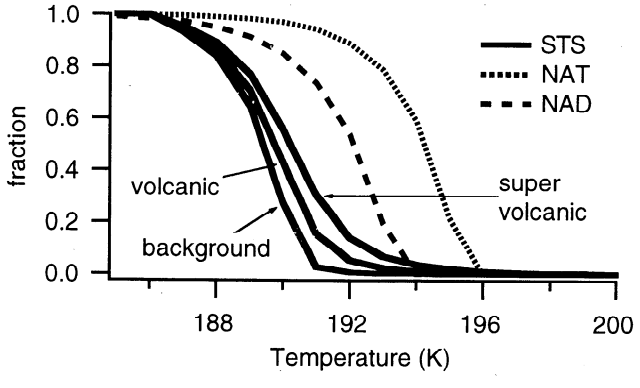

Figure 6. Plot of the fraction of total HNO_3 incorporated into particles for several particle types as a function of temperature. This quantity is comparable to that plotted in Figure 3. Pressure is set at each temperature in order to maintain the potential temperature at 465 K.

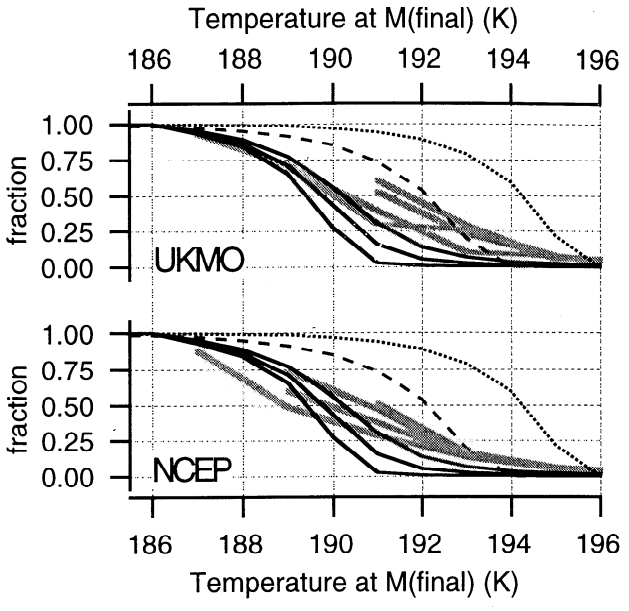

Figure 7. Comparison of observed depletion of HNO_3 from Figure 3 (gray lines) and the model depletion from Figure 6 (black lines: solid, STS; dashed, NAD; dotted, NAT).

Using a Monte Carlo analysis, we determine the uncertainty in the model curves due to uncertainty in the assumptions of HNO_3, H_2O, and H_2SO_4 to be ±1 K (1σ) along the x axis (this means that changes in the inputs to the model could shift the curve by as much as ±1 K along the x axis). The uncertainty in the model curves due to errors in the parameterization of p_{HNO3} (the vapor pressure of HNO_3 above these particles) is estimated to be ±50% for STS [*Carslaw et al.*, 1997, section 6], and ±35% and 65% for NAT and NAD, respectively [*Del Negro et al.*, 1997]. This translates into an additional uncertainty in the model curves of ~±1.5 K along the x axis. Combining these errors, we estimate the total uncertainty in the model curves to be ~±2 K.

Figure 7 shows a comparison of observed denitrification from Figure 3 and the models from Figure 6. In general, the observations show a more gradual increase in denitrification with decreasing temperature than the models predict. This behavior is likely at least partially due to the rather large atmospheric volume from which the measurement is averaged: several hundred kilometers by ~10 km in the horizontal, and ~5 km in the vertical. Temperature inhomogeneities in the volume would tend to smear out any sharp edges in the temperature dependence of the observed denitrification.

The observations fall between the NAD and STS lines, and far away from the NAT curves. When assessing this comparison, it is crucial to recognize that both UKMO and

NCEP temperature fields, from which the temperatures in this analysis are determined, have warm biases. Comparisons with radiosonde measurements show that Northern Hemisphere UKMO temperatures are warm biased by 1-4 K for temperatures below 200 K, while the NCEP temperatures are warm biased by 0.5-2 K [*Manney et al.*, 1996, Table 1]. Taking these biases into account would shift the observations to the left (i.e., to lower temperatures), generally improving agreement between the observations and the STS models and worsening the agreement with the NAT and NAD models.

We conclude that the STS model best describes these Northern Hemisphere observations. Other analyses [e.g., *Drdla et al.*, 1994; *Toon and Tolbert*, 1995; *Massie et al.*, 1997; *Dye et al.*, 1996; *Santee et al.*, 1998], utilizing different methodologies, have also come to this conclusion. Taking the various sources of uncertainty into account, we cannot, however, rule out NAD as a possible form. Because of the poor agreement between the NAT model and the observations, we believe that our analysis provides no evidence in support of NAT as an important component of type I PSCs.

There are several caveats to these conclusions. First, our analysis is an average over the entire winter/early spring time period. *Santee et al.* [1998] argue that in the Southern Hemisphere, STS is more important early in the winter, and NAD becomes more important later. Because of our need to average many observations of HNO_3, we cannot address questions about the relative importance of the various PSC forms as a function of time during the winter. Second, the vertical resolution of the measurement is ~5 km for version 4 MLS HNO_3, and so we have no information about the distribution of HNO_3 within the measurement volume. As a result, we cannot distinguish a slight uniform decrease of HNO_3 over the entire vertical extent of the measurement from a massive decrease of HNO_3 over a thin layer. Consequently, our results must be considered suggestive of the importance of STS, but not conclusive.

The eruption of Mount Pinatubo significantly increased the abundance of stratospheric H_2SO_4 immediately following the eruption in mid 1991 [*Bluth et al.*, 1992; *McCormick and Veiga*, 1992]. The lifetime of such a perturbation is 1-2 years [*McCormick et al.*, 1995], so we expect the abundance of stratospheric H_2SO_4 to be decreasing significantly during the time period spanned by Figure 3 (1991-1996). From Figure 6 we see that STS particles take up HNO_3 more efficiently at a given temperature when H_2SO_4 is high. Figure 3 shows that, at a given temperature, denitrification was greater in 1991-1992 and 1992-1993 than in later years, consistent with higher H_2SO_4 abundances during the early years. We conclude, therefore, that the interannual variability observed is consistent with our identification of STS as the dominant form of type I PSC.

Figure 8 shows a plot similar to Figure 7, but for the Antarctic winters of 1992, 1993, and 1994. It should be noted that the requirement that the $M_{initial}$ measurements be made at $T > 196$ K limits the Antarctic observation period to between late May and late June. After that, the vortex temperatures are rarely above 196 K. Given similar model-curve uncertainties and similar warm biases for the temperatures [*Manney et al.*, 1996, Table 2], we conclude again

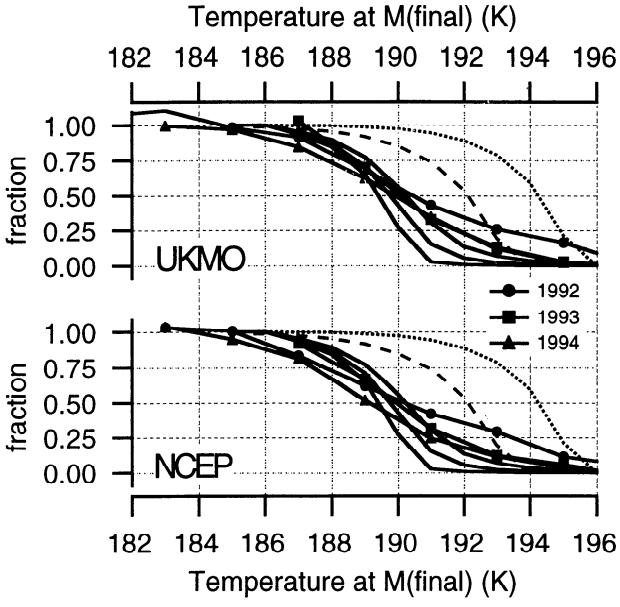

Figure 8. Ratio of average $M_{initial}$-M_{final} HNO_3 to average $M_{initial}$ HNO_3 plotted against the temperature of the air mass at the M_{final} location for the Southern Hemisphere. Analyses were run at 465-K potential temperature (~20 km), and between June 12 and June 30, 1992, and May 20 and June 30 of 1993 and 1994. Winds and temperatures are from (top) the UKMO and (bottom) the NCEP.

that the STS model best describes the observations. Owing to uncertainty in our analysis, we cannot rule out NAD as a possible form for type I PSCs. Our analysis provides no evidence to support NAT as a possible form for type I PSCs.

The observations of denitrification in the Southern Hemisphere are similar to those in the Northern Hemisphere shown in Figure 3. This suggests that the vapor pressure of HNO_3 over the particles (and therefore the composition of the particles) in the two hemispheres is similar. The interannual variability of the observations is also consistent with the enhanced sulfate loading caused by the eruption of Mount Pinatubo, with the 1992 observations showing higher levels of denitrification than other years. Finally, agreement between the UKMO and NCEP analyses is good.

4. Irreversible Denitrification

The analysis in the last section showed that as the temperature of an air parcel is lowered below ~196 K, HNO_3 is removed from the gas phase. The analysis did not tell us, however, if the denitrification was temporary or irreversible. We address this issue in this section.

To study irreversible denitrification, we identify measurements made in the same air mass several days apart, all at temperatures above 196 K. We then find those air trajectories that experienced low temperatures in the intervening time. By comparing the HNO_3 abundance before and after the cold event, we can determine if any irreversible denitrification occurred.

To do this, UARS data from an initial day are interpolated to the 465-K potential temperature surface (~20 km)

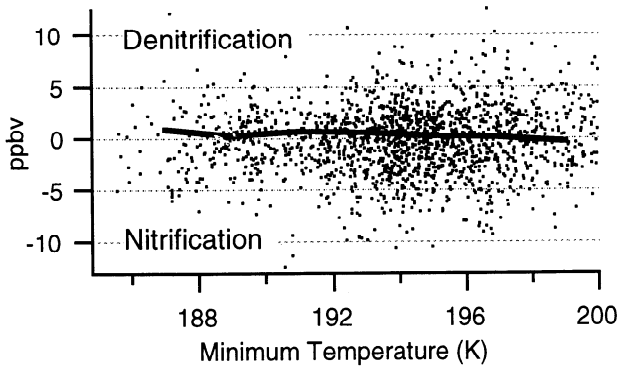

Figure 9. $M_{initial}$-M_{final} HNO_3 versus minimum temperature of the air mass during the trajectory (dots), and $M_{initial}$-M_{final} HNO_3 sorted into 2-K minimum-temperature bins and averaged (solid line). The analysis was run at 465-K potential temperature (~20 km), and between December 12, 1995 and March 28, 1996. Winds and temperatures are from the UKMO. Negative values imply nitrification, where HNO_3 increases along the trajectory.

and advected forward using the trajectory model to 0000UT of the fourth day following. For example, if the initial day is January 9, then the measurements are advected to midnight between January 12 and January 13 (0000UT January 13). UARS data from the four days following this stopping time (in this case, January 13-16) are advected backward to this same stopping time. In all cases, only UARS measurements made at temperatures above 196 K and latitudes poleward of 60° are used, on the basis of the assumption that such air will be PSC-free and all of the parcels' HNO_3 will be in the gas phase. As in the previous section, we assume that trajectories that are "near" each other at the common stopping time indicate that the measurements associated with these parcels were made in the same air mass. We use the same criteria for "near" as in the previous analysis.

We define the measurements made on the initial day (in our example, January 9) as $M_{initial}$. For each $M_{initial}$ value, we isolate those measurements from the later four days (January 13-16) that are in the same air mass as the $M_{initial}$ value and define the average of these data as M_{final}.

We now investigate the change in HNO_3 abundance during the trajectory. Figure 9 shows $M_{initial}$ - M_{final} HNO_3 abundance plotted against the minimum temperature along the trajectory for individual trajectories (dots), as well as an average line. Most of the HNO_3 that is taken up by the PSCs (as shown in Figure 3) is returned to the gas phase when the air mass warms up.

Figure 10 shows the average line from Figure 9 as well as the lines from other years, and lines calculated using the NCEP winds and temperatures. If we assume that irreversible denitrification does not occur on trajectories that do not reach minimum temperatures below 196 K, then the scatter at these temperatures provides an estimate of the uncertainty of this method to be ~±0.5 ppbv.

In general, $M_{initial}$ - M_{final} HNO_3 is less than our estimate of the total error (±0.5 ppbv) for minimum temperatures above 190 K, suggesting little, if any, irreversible denitrification occurring at these temperatures. At minimum temperatures below 190 K, $M_{initial}$ - M_{final} HNO_3 increases to 0.5 to 2 ppbv. This difference is larger than our estimate of total error, suggesting that some irreversible denitrification is occurring at these low temperatures. It should be noted that this irreversible denitrification is statistically significant: the standard error of the mean at these temperatures is ~0.5 ppbv.

Figure 10 shows 0.5 to 2 ppbv of irreversible denitrification occurring every time the minimum temperature of a Northern Hemispheric air mass drops below 190 K. Given HNO_3 abundances of ~12 ppbv, this corresponds to irreversible denitrification of 4-17% of HNO_3. Note that disagreements between the UKMO- and NCEP-based analyses, as well as large year-to-year variability, make the total uncertainty of our estimate significant. In light of this, we believe it is most appropriate to conclude that our analysis suggests an upper limit of irreversible denitrification to be 17% per cold event (where a "cold event" is one in which the air mass temperature drops below 190 K), but could also be consistent with no irreversible denitrification. It should also be remembered that this value is an average for the entire winter. Our analysis sheds no light on the distribution of irreversible denitrification amounts of the individual trajectories that make up the average.

What is not seen in Figure 10 is as important as what is seen. We see no evidence that a single exposure to low temperatures will irreversibly remove a significant fraction of the HNO_3 from an air mass, even at temperatures close to the frost point. Consequently, our analysis suggests that in order to remove a significant fraction of the HNO_3 from an air mass in the Northern Hemisphere, one must expose it to cold temperatures several times.

In order to conclude that the change in HNO_3 abundance seen below 190 K represents irreversible denitrification, we have to assume that all of the HNO_3 is in the gas phase at

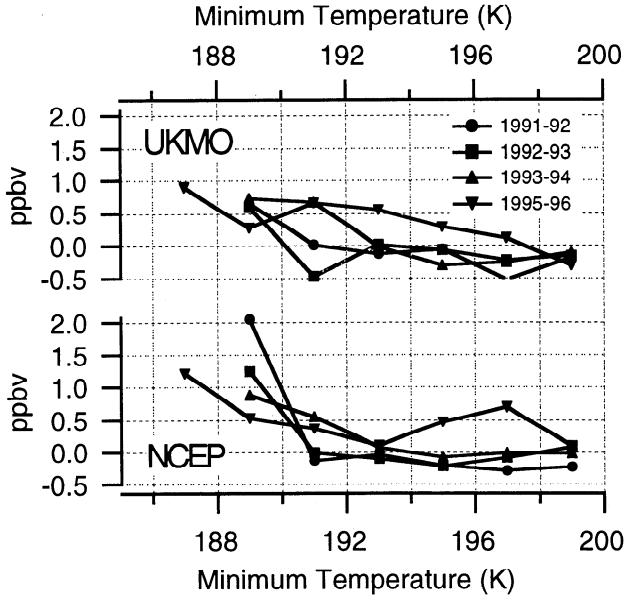

Figure 10. Average $M_{initial}$-M_{final} HNO_3 plotted against the minimum temperature along the trajectory. Analyses were run at 465-K potential temperature (~20 km), and between December 12 and March 28 of the years indicated. Winds and temperatures are from (top) the UKMO and (bottom) the NCEP.

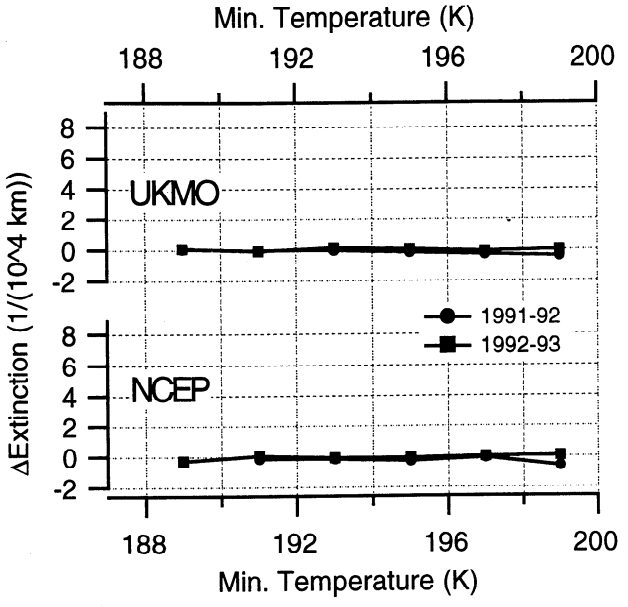

Figure 11. Average M_{final} - $M_{initial}$ extinction (at 780 cm^{-1}) plotted against minimum temperature along the trajectory. Analyses were run at 465-K potential temperature (~20 km), and between December 12 and March 28 of the years indicated. Winds and temperatures are from (top) the UKMO and (bottom) the NCEP. The scale of the *y* axis is set to be the same as in Figure 5 in order to highlight the differences between them.

both the $M_{initial}$ and M_{final} points. If this were not true, then a deficit in HNO_3 at M_{final} could also be explained by the fact that some of the HNO_3 was still tied up in small particles that have not evaporated yet. To address this, in Figure 11 we perform the same analysis as in Figure 10, but using extinction measured by the CLAES. Comparison with Figure 5 shows that the enhanced extinction observed at low temperatures disappears when the parcel warms up. We conclude that there is no evidence to support the idea that any HNO_3 is tied up in particles at M_{final}, and therefore the decrease in HNO_3 between the $M_{initial}$ and M_{final} locations represents irreversible denitrification.

The method of quantifying irreversible denitrification that we use in this paper requires $M_{initial}$ and M_{final} measurements to occur at temperatures greater than 196 K and within 7 days of each other. This requirement constrains the events that we can observe: air parcels that experience temperatures below 196 K for longer periods cannot be considered by this method and are therefore not included in Figures 9 through 11. Trajectories initialized in the vortex and run for the entire winter indicate that about 10-15% of the trajectories whose temperatures drop below 196 K will maintain temperatures below 196 K for longer than 7 days. It is possible that these trajectories are experiencing significant irreversible denitrification; our analysis sheds no light on this. However, we can say that these trajectories spend much of their time just below the 196-K threshold. Only about 1% of the trajectories that drop below 194 K will maintain temperatures below 194 K for longer than 7 days. More research on these persistently cold trajectories is needed to positively determine their contribution to the NO_y budget of the polar vortex.

Another result of our 7-day constraint is that we have no observations of irreversible denitrification for the Southern Hemisphere. Because the temperature in the Southern Hemisphere polar vortex is rapidly dropping over this time period, once the temperature of an air parcel drops below ~196 K, the temperature tends to stay below 196 K for more than 7 days. Therefore our method finds few Southern Hemisphere vortex trajectories where both ends of the trajectory are at temperatures above 196 K. As a result, we show no observations of irreversible denitrification in the Southern Hemisphere.

Virtually all previous analyses of irreversible denitrification have used a "conservative coordinate" approach [e.g., *Fahey et al.*, 1990b; *Rinsland et al.*, 1999; *Sugita et al.*, 1998; *Hintsa et al.*, 1998]. This method relies on measuring NO_y changes relative to a constituent that is considered conserved, usually N_2O. Any decrease in NO_y relative to a reference NO_y-N_2O correlation is attributed to irreversible denitrification. *Rinsland et al.* [1999] use Atmospheric Trace Molecule Spectroscopy (ATMOS) data to estimate that irreversible denitrification in the northern hemisphere removed 5±2 ppbv (~30%) of NO_y at ~470 K in the polar region in 1993. *Sugita et al.* [1998] estimate that irreversible denitrification in the northern hemisphere removed ~70% of the NO_y at 19.5 km (close to the 465-K level investigated in this paper) in the polar air mass that their balloon flew through.

There are, however, difficulties associated with this approach. Foremost is separating changes in the correlation caused by mixing in of air from midlatitudes [e.g., *Strahan et al.*, 1996] from changes due to irreversible denitrification. Using similar data sets, *Michelsen et al.* [1998], *Kondo et al.* [1999], and M. Rex et al. (Subsidence, mixing and denitrification of Arctic polar vortex air measured during POLARIS, submitted to *Journal of Geophysical Research,* 1999) argue that most of the apparent denitrification of the *Rinsland et al.* [1999] and *Sugita et al.* [1998] papers can be attributed to the combination of descent in the polar vortex and mixing into the vortex of midlatitude air.

Other analyses, emphasizing regions with N_2O abundances > 100 ppbv, suggest irreversible denitrification is occurring in the north. *Hintsa et al.* [1998] showed evidence of irreversible denitrification of >50% occurring over a ~1-km-thick layer in 1996. *Fahey et al.* [1990a] also show significant irreversible denitrification in February 1989. Based on this, it seems that irreversible denitrification does occur, but with significant interannual variability. Finally, this conservative-coordinate approach only determines the integrated loss in an air parcel between the time the reference correlation is obtained and the subsequent measurements. Our analysis suggests that the average irreversible denitrification during a single exposure to cold temperatures is small, less than 17%. Significant denitrification could occur, however, from multiple exposures to temperatures near the frost point.

5. Conclusions

We have presented measurements of temporary and irreversible denitrification. Averaging observations over an

entire winter period, we find that our observations of the uptake of HNO_3 by particles in both hemispheres are best described by a supercooled ternary solution (STS) model. Considering the uncertainties in the analysis, our results are also consistent with a nitric acid dihydrate (NAD) composition for type I PSCs, but not a nitric acid trihydrate (NAT) composition. The similarity of the temperature dependence of the denitrification between the two hemispheres suggests that the composition of the type I PSCs is at least approximately the same in the northern and southern polar vortices.

We observe irreversible denitrification in the Northern Hemisphere of as much as 17% of the HNO_3 occurs each time the temperature of the trajectory drops below 190 K. Due to uncertainties in our analysis, this figure must be considered an upper limit. Finally, while difficult to compare, our work is not inconsistent with previous observations of irreversible denitrification. Occurrences of large denitrification could be caused by multiple exposures to temperatures near the frost point.

Acknowledgments. We thank contributions from D. B. Considine, S. R. Kawa, G. L. Manney, H. A. Michelsen, and J. M. Pierson. We thank C. P. Rinsland and Y. Kondo for providing preprints of their work. This work was supported by UARS guest investigator grants to NASA GSFC and the University of Maryland.

References

Anderson, J. G., D. W. Toohey, and W. H. Brune, Free radicals within the Antarctic vortex: The role of CFCs in Antarctic ozone loss, *Science, 251,* 39-46, 1991.

Bluth, G. J. S., S. D. Doiron, C. C. Schnetzler, A. J. Krueger, and L. S. Walter, Global tracking of the SO_2 clouds from the June, 1991 Mount Pinatubo eruptions, *Geophys. Res. Lett., 19,* 151-154, 1992.

Brune, W. H., J. G. Anderson, D. W. Toohey, D. W. Fahey, S. R. Kawa, R. L. Jones, D. S. McKenna, and L. R. Poole, The potential for ozone depletion in the Arctic polar stratosphere, *Science, 252,* 1260-1266, 1991.

Carslaw, K. S., B. P. Luo, and T. Peter, An analytic expression for the composition of aqueous HNO_3-H_2SO_4 stratospheric aerosols including gas-phase removal of HNO_3, *Geophys. Res. Lett., 22,* 1877-1880, 1995.

Carslaw, K. S., T. Peter, and S. L. Clegg, Modeling the composition of liquid stratospheric aerosols, *Rev. Geophys., 35,* 125-154, 1997.

Del Negro, L. A., et al., Evaluating the role of NAT, NAD, and liquid $H_2SO_4/H_2O/HNO_3$ solutions in Antarctic polar stratospheric cloud aerosol: Observations and implications, *J. Geophys. Res., 102,* 13,255-13,282, 1997.

Dessler, A. E., D. B. Considine, G. A. Morris, M. R. Schoeberl, A. E. Roche, J. L. Mergenthaler, J. M. Russell, J. W. Waters, J. C. Gille, and G. K. Yue, Correlated observations of HCl and $ClONO_2$ from UARS and implications for stratospheric chlorine partitioning, *Geophys. Res. Lett., 22,* 1721-1724, 1995.

Dessler, A. E., M. D. Burrage, J.-U. Grooß, J. R. Holton, J. L. Lean, S. T. Massie, M. R. Schoeberl, A. R. Douglass, and C. H. Jackman, Selected science highlights from the first five years of the Upper Atmosphere Research Satellite (UARS) program, *Rev. Geophys., 36,* 183-210, 1998.

Drdla, K., and R. P. Turco, Denitrification through PSC formation: A 1-D model incorporating temperature oscillations, *J. Atmos. Chem., 12,* 319-366, 1991.

Drdla, K., A. Tabazadeh, R. P. Turco, M. Z. Jacobson, J. E. Dye, C. Twohy, and D. Baumgardner, Analysis of the physical state of one Arctic polar stratospheric cloud based on observations, *Geophys. Res. Lett., 21,* 2475-2478, 1994.

Dye, J. E., et al., In-situ observations of an Antarctic polar stratospheric cloud: Similarities with Arctic observations, *Geophys. Res. Lett., 23,* 1913-1916, 1996.

Fahey, D. W., K. K. Kelly, G. V. Ferry, L. R. Poole, J. C. Wilson, D. M. Murphy, M. Loewenstein, and K. R. Chan, In situ measurements of total reactive nitrogen, total water, and aerosol in a polar stratospheric cloud in the Antarctic, *J. Geophys. Res., 94,* 11,299-11,315, 1989.

Fahey, D. W., K. K. Kelly, S. R. Kawa, A. F. Tuck, M. Loewenstein, K. R. Chan, and L. E. Heidt, Observations of denitrification and dehydration in the winter polar stratospheres, *Nature, 344,* 321-324, 1990a.

Fahey, D. W., S. Solomon, S. R. Kawa, M. Loewenstein, J. R. Podolske, S. E. Strahan, and K. R. Chan, A diagnostic for denitrification in the winter polar stratosphere, *Nature, 345,* 698-702, 1990b.

Hanson, D., and K. Mauersberger, Laboratory studies of the nitric acid trihydrate: Implications for the south polar stratosphere, *Geophys. Res. Lett., 15,* 855-858, 1988.

Hintsa, E. J., et al., Dehydration and denitrification in the Arctic polar vortex during the 1995-1996 winter, *Geophys. Res. Lett., 25,* 501-504, 1998.

Kawa, S. R., D. W. Fahey, L. E. Heidt, W. H. Pollock, S. Solomon, D. E. Anderson, M. Loewenstein, M. H. Proffitt, J. J. Margitan, and K. R. Chan, Photochemical partitioning of the reactive nitrogen and chlorine reservoirs in the high-latitude stratosphere, *J. Geophys. Res., 97,* 7905-7923, 1992a.

Kawa, S. R., D. W. Fahey, K. K. Kelly, J. E. Dye, D. Baumgardner, B. W. Gandrud, M. Loewenstein, G. V. Ferry, and K. R. Chan, The Arctic polar stratospheric cloud aerosol: Aircraft measurements of reactive nitrogen, total water, and particles, *J. Geophys. Res., 97,* 7925-7938, 1992b.

Kondo, Y., P. Aimedieu, M. Koike, Y. Iwasaka, P. A. Newman, U. Schmidt, W. A. Matthews, M. Hayashi, and W. R. Sheldon, Reactive nitrogen, ozone, and nitrate aerosols observed in the Arctic stratosphere in January 1990, *J. Geophys. Res., 97,* 13,025-13,038, 1992.

Kondo, Y., et al., NO_y-N_2O correlation observed inside the Arctic vortex in February 1997: Dynamical and chemical effects, *J. Geophys. Res.,* in press, 1999.

Manney, G. L., R. Swinbank, S. T. Massie, M. E. Gelman, A. J. Miller, R. Nagatani, A. O'Neill, and R. W. Zurek, Comparison of U.K. Meteorological Office and U.S. National Meterological Center stratospheric analyses during northern and southern winter, *J. Geophys. Res., 101,* 10,311-10,334, 1996.

Massie, S. T., et al., Validation studies using multiwavelength Cryogenic Limb Array Etalon Spectrometer (CLAES) observations of stratospheric aerosol, *J. Geophys. Res., 101,* 9757-9773, 1996.

Massie, S. T., et al., Simultaneous observations of polar stratospheric clouds and HNO_3 over Scandanavia in January, 1992, *Geophys. Res. Lett., 24,* 595-598, 1997.

McCormick, M. P., and R. E. Veiga, SAGE II measurements of early Pinatubo aerosols, *Geophys. Res. Lett., 19,* 155-158, 1992.

McCormick, M. P., L. W. Thomason, and C. R. Trepte, Atmospheric effects of the Mt Pinatubo eruption, *Nature, 373,* 399-404, 1995.

Michelsen, H. A., G. L. Manney, M. R. Gunson, and R. Zander, Correlations of stratospheric $[NO_y]$, $[O_3]$, $[N_2O]$, and $[CH_4]$ derived from ATMOS measurements, *J. Geophys. Res., 103,* 28,347-28,359, 1998.

Morris, G. A., et al., Trajectory mapping and applications to data from the Upper Atmosphere Research Satellite, *J. Geophys. Res., 100,* 16,491-16,505, 1995.

Morris, G. A., D. B. Considine, A. E. Dessler, S. R. Kawa, J. B. Kumer, J. L. Mergenthaler, A. E. Roche, and J. M. Russell, III, Nitrogen partitioning in the middle stratosphere as observed by the Upper Atmosphere Research Satellite, *J. Geophys. Res., 102,* 8955-8965, 1997.

Panegrossi, G., D. Fuà, and G. Fiocco, A 1-D model of the formation and evolution of polar stratospheric clouds, *J. Atmos. Chem., 23,* 5-35, 1996.

Peter, T., Microphysics and heterogeneous chemistry of polar stratospheric clouds, *Ann. Rev. Phys. Chem., 48,* 785-822, 1997.

Rinsland, C. P., R. J. Salawitch, M. R. Gunson, S. Solomon, R. Zander, E. Mahieu, A. Goldman, M. J. Newchurch, F. W. Irion, and A. Y. Chang, Polar stratospheric descent of NO_y and CO and Arctic denitrification during winter 1992-93, *J. Geophys. Res., 104,* 1847-1861, 1999.

Salawitch, R. J., et al., Chemical loss of ozone in the Arctic polar vortex in the winter of 1991-1992, *Science, 261,* 1146-1149, 1993.

Santee, M. L., W. G. Read, J. W. Waters, L. Froidevaux, G. L. Manney, D. A. Flower, R. F. Jarnot, R. S. Harwood, and G. E. Peckham, Interhemispheric differences in polar stratospheric HNO_3, H_2O, ClO, and O_3, *Science, 267,* 849-852, 1995.

Santee, M. L., G. L. Manney, W. G. Read, L. Froidevaux, and J. W. Waters, Polar vortex conditions during the 1995-96 Arctic winter: MLS ClO and HNO_3, *Geophys. Res. Lett., 23,* 3207-3210, 1996.

Santee, M. L., G. L. Manney, L. Froidevaux, R. W. Zurek, and J. W. Waters, MLS observations of ClO and HNO_3 in the 1996-97 Arctic polar vortex, *Geophys. Res. Lett., 24,* 2713-2716, 1997.

Santee, M. L., A. Tabazadeh, G. L. Manney, R. J. Salawitch, L. Froidevaux, W. G. Read, and J. W. Waters, UARS MLS HNO_3 observations: Implications for Antarctic PSCs, *J. Geophys. Res., 103,* 13,285-13,313, 1998.

Schoeberl, M. R., and L. C. Sparling, Trajectory modelling, in *Diagnostic Tools in Atmospheric Physics, Proceedings of the International School of Physics,* edited by G. Fiocco and G. Visconti, pp. 289-305, IOS Press, Amsterdam, 1995.

Solomon, S., Progress towards a quantitative understanding of Antarctic ozone depletion, *Nature, 347,* 347-354, 1990.

Strahan, S. E., J. E. Nielsen, and M. C. Cerniglia, Long-lived tracer transport in the Antarctic stratosphere, *J. Geophys. Res., 101,* 26,615-26,629, 1996.

Sugita, T., Y. Kondo, H. Nakajima, U. Schmidt, A. Engel, H. Oelhaf, G. Wetzel, M. Koike, and P. A. Newman, Denitrification observed inside the Arctic vortex in February 1995, *J. Geophys. Res., 103,* 16,221-16,233, 1998.

Swinbank, R., and A. O'Neill, A stratosphere-troposphere data assimilation system, *Mon. Weather Rev., 122,* 686-702, 1994.

Tabazadeh, A., R. P. Turco, K. Drdla, M. Z. Jacobson, and O. B. Toon, A study of type I polar stratospheric cloud formation, *Geophys. Res. Lett., 21,* 1619-1622, 1994.

Toon, O. B., E. V. Browell, S. Kinne, and J. Jordan, An analysis of LIDAR observations of polar stratospheric clouds, *Geophys. Res. Lett., 17,* 393-396, 1990.

Toon, O. B., and M. A. Tolbert, Spectroscopic evidence against nitric acid trihydrate in polar stratospheric clouds, *Nature, 375,* 218-221, 1995.

Weisenstein, D. K., G. K. Yue, M. K. W. Ko, N.-D. Sze, J. M. Rodriguez, and C. J. Scott, A two-dimensional model of sulfur species and aerosols, *J. Geophys. Res., 102,* 13,019-13,035, 1997.

World Meteorological Organization, Scientific assessment of ozone depletion: 1994, *WMO Rep. 37,* Global Ozone Res. and Monit. Proj., Geneva, 1995.

Worsnop, D. R., L. E. Fox, M. S. Zahniser, and S. C. Wofsy, Vapor pressures of solid hydrates of nitric acid: Implications for polar stratospheric clouds, *Science, 259,* 71-74, 1993.

A. E. Dessler and J. Wu, Department of Meteorology, University of Maryland, College Park, MD 20742 (dessler@atmos.umd.edu).

M. L. Santee, NASA Jet Propulsion Laboratory, Mail Stop 183-701, 4800 Oak Grove Drive, Pasadena, CA 91109-8099.

M. R. Schoeberl, Code 910, NASA Goddard Space Flight Center, Greenbelt, MD 20771.

(Received October 26, 1998; revised February 17, 1999; accepted February 23, 1999.)